American Mineralogist, Volume 83, pages 491–500, 1998

Melting experiments in the systems $CaO-MgO-Al_2O_3-SiO_2$ and $MgO-SiO_2$ at 3 to 15 GPa

CLAUDE HERZBERG[1,*] AND JIANZHONG ZHANG[2]

[1]Department of Geological Sciences, Rutgers University, New Brunswick, New Jersey 08903, U.S.A.
[2]Center for High Pressure Research and Mineral Physics Institute, The State University of New York, Stony Brook, New York 11794, U.S.A.

ABSTRACT

The results of multi-anvil melting experiments are reported for a range of compositions in the system $CaO-MgO-Al_2O_3-SiO_2$. The liquidus crystallization fields for forsterite, orthopyroxene, clinopyroxene, and garnet have been mapped out at 10 GPa, as have their intersections at various cotectics. The composition of the liquid that is multiply saturated in forsterite, orthopyroxene, clinopyroxene, and garnet has been also determined to within ± 0.5–1.0 wt% (2σ), and the result is in excellent agreement with a previous estimate (Herzberg 1992). These experiments confirm that the effect of pressure is to reduce Al_2O_3 and increase MgO and SiO_2 in magmas formed by the melting of garnet lherzolite with increasing pressure (Herzberg 1992). Melting experiments in the system $MgO-SiO_2$ also have been performed to constrain how pressure affects the compositions of liquids that are saturated in harzburgite [L + Ol + Opx]. Experiments in both $CaO-MgO-Al_2O_3-SiO_2$ and $MgO-SiO_2$ demonstrate that there is a maximum normative olivine content to liquids formed by initial or advanced melting of peridotite in the upper mantle, and this occurs at 7 to 8 GPa. For most peridotites that undergo decompression melting in a plume, clinopyroxene and garnet are the first crystalline phases to melt out and, with a few important but rare exceptions, the experimentally constrained liquids are unlike most volcanic rocks. Advanced anhydrous melting will yield liquids with a residual harzburgite mineralogy [L + Ol + Opx], and these liquids are similar in composition to most komatiites with Cretaceous and 2700 Myr Archaean ages.

INTRODUCTION

In a companion paper (Herzberg and Zhang 1997), we demonstrated that it was possible to constrain the compositions of liquids at invariant points and cotectics in the system $CaO-MgO-Al_2O_3-SiO_2$ (CMAS) at 5 GPa with a precision and accuracy that is comparable to experiments at low pressures (i.e., ± 0.5–1.0% 2σ). Those experiments were carried out in a multi-anvil apparatus wherein the liquid compositions were bracketed by examining the liquidus phases for a wide range of compositions, namely the ''shotgun'' method. Similar experiments have been carried on oxide mixes in the system CMAS at 10 GPa using an identical experimental method, and the results are reported here.

The experiments reported here are important for determining the compositions of magmas produced by initial melting of garnet lherzolite at high pressures [Liquid + Olivine + Orthopyroxene + Clinopyroxene + Garnet]. Previous experimental work (Herzberg 1992, 1995; Herzberg and O'Hara unpublished manuscript) showed that all clinopyroxene and garnet can be dissolved during advanced melting on decompression. The liquids that erupt solidify to picrites and komatiites, and most of these rocks have a major element composition that can be described by the partial melting of peridotite with a residual harzburgite mineralogy [L + Ol + Opx]. These interpretations have been confirmed by the experiments reported here. But to better understand the

TABLE 1. Compositions of oxide mix starting materials (wt%)

Mix	SiO_2	Al_2O_3	MgO	CaO
27	51.20	4.20	36.80	7.80
28	52.20	4.20	35.80	7.80
29	52.78	0.00	47.22	0.00
30	54.39	0.00	45.61	0.00
31	51.40	3.77	36.60	8.23
32	51.40	3.50	36.35	8.75
33	48.58	5.03	35.42	10.97
34	47.99	4.53	37.61	9.87
35	48.39	6.04	35.15	10.42
37	53.59	0.00	46.41	0.00
38	55.15	0.00	44.85	0.00
39	55.89	0.00	44.11	0.00
C*	50.25	5.06	40.88	3.81
C67†	53.14	3.37	39.12	4.37
C50‡	54.58	2.53	38.23	4.66

* Herzberg et al. (1990).
† Herzberg (1992).
‡ All mixes total to 100%.

* E-mail: herzberg@rci.rutgers.edu

0003–004X/98/0506–0491$05.00

TABLE 2. Experimental results

Mix no.-Experiment no.	27-1	28-1	29-1	29-2
T (°C)	2070	2070	2100	1875
P (GPa)	10	10	10	5
Time (min)	7	7	7	15
Crystallization sequence	L L + Gt L + Gt + Fo + Opx L + Gt + Fo + Cpx [Gt + Fo + Cpx]	L L + Gt L + Gt + Opx L + Gt + Fo + Cpx [Gt + Cpx + Fo]	L L + Fo L + Fo + En [Fo + En]	L L + Fo L + Fo + En [Fo + En]
Mix no.-Experiment no.	30-1	30-2	30-3	30-4
T (°C)	2100	1850	2200	2225
P (GPa)	10	5	15	12
Time (min)	7	15	10	7
Crystallization sequence	L L + En L + En + Fo [En + Fo]	L L + En L + En + Fo [En + Fo]	L L + En L + En + Fo [En + Fo]	L L + Fo L + Fo + En [Fo + En]
Mix no.-Experiment no.	31-1	32-1	33-1	34-1
T (°C)	2020	2020	2020	2020
P (GPa)	10	10	10	10
Time (min)	7	7	7	7
Crystallization sequence	L L + Opx + Fo + Gt + Cpx [Fo + Gt + Cpx]	L L + Fo + Cpx L + Fo + Cpx + Gt [Fo + Cpx + Gt]	L L + Gt L + Gt + Fo L + Gt + Fo + Cpx [Gt + Fo + Cpx]	L L + Fo L + Fo + Gt L + Fo + Gt + Cpx [Fo + Gt + Cpx]
Mix no.-Experiment no.	35-1	37-1	37-2	37-3
T (°C)	2020	2100	1850	2200
P (GPa)	10	10	5	15
Time (min)	5	7	12	10
Crystallization sequence	L L + Gt L + Gt + Fo L + Gt + Fo + Cpx [Gt + Fo + Cpx]	L L + Fo L + Fo + En [Fo + En]	L L + En L + En + Fo [En + Fo]	L L + En + minor Fo L + En + Fo [En + Fo]
Mix no.-Experiment no.	38-1	38-2	38-3	39-1
T (°C)	1850	1800	2195	1850
P (GPa)	5	3	12	5
Time (min)	15	20	10	15
Crystallization sequence	L L + En L + En + Fo [En + Fo]	L L + Fo L + Fo + En [Fo + En]	L L + Fo + En [Fo + En]	L L + En L + En + Fo [En + Fo]
Mix no.-Experiment no.	39-2	C*	C67†	C50†
T (°C)	2225	2080	2070	2080
P (GPa)	12	10	10	10
Time (min)	10	5	3	4
Crystallization sequence	L L + En L + En + Fo [En + Fo]	L L + Fo + Gt L + Fo + Gt + Opx L + Fo + Gt + Opx + Cpx	L L + Opx L + Opx + Fo L + Opx + Fo + Gt L + Opx + Fo + Gt + Cpx	L L + Opx L + Opx + Fo L + Opx + Fo + Gt + Cpx

Notes: L = Liquid; Fo = Forsterite; Opx = Orthopyroxene; Cpx = Clinopyroxene; Gt = Garnet; En = Enstatite; phases in square parentheses = subsolidus phases.

* Herzberg et al. (1990).

† Herzberg (1992).

melting of peridotite with a harzburgite residuum, we also report the results of experiments performed on compositions in the system Forsterite (Mg_2SiO_4)-Enstatite ($Mg_2Si_2O_6$).

EXPERIMENTAL METHOD

The experimental method adopted here is identical to the one used in our companion study (Herzberg and Zhang 1997), and the reader is referred to that paper for a detailed discussion. An important question is the best experimental method for accurately determining the composition of a liquid at the invariant point of interest, that being [L + Fo + Opx + Cpx + Gt] at 10 GPa. Following on our previous success, we have adopted the ''shotgun'' technique wherein the liquid composition is bracketed by observing the liquidus phase for a range of bulk compositions. In the ideal case, if the bulk composition is the same as the peritectic liquid, the experiment will exhibit multiple saturation in the maximum number of crystalline phases as we report for the first time in this paper. An important reason for adopting the ''shotgun'' technique has arisen from problems associ-

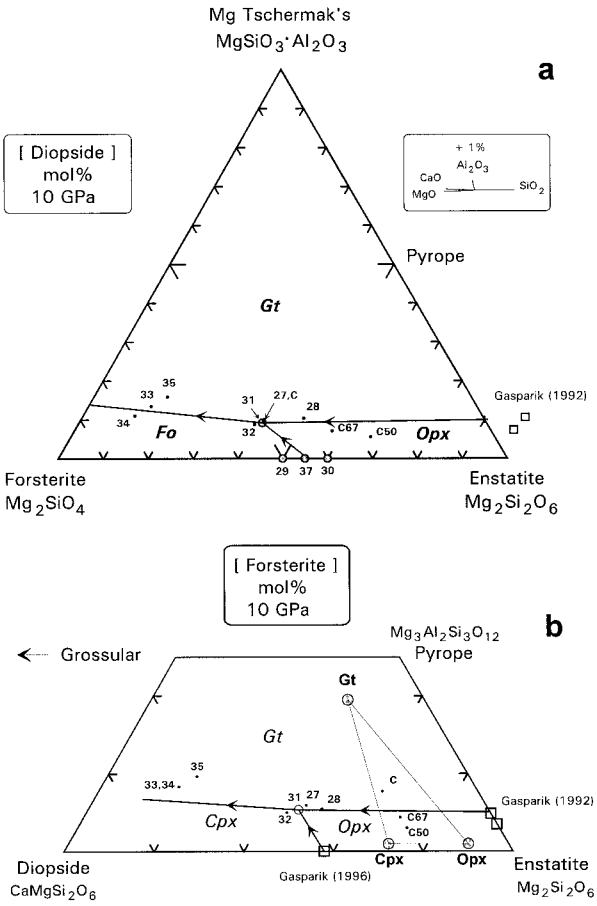

FIGURE 1. Projections of experimental oxide mixes, liquidus phase boundaries, and coexisting garnet, clinopyroxene and orthopyroxene at 10 GPa. **(a)** From Diopside onto the plane Fo-En-Mg Tschermak's. **(b)** From Forsterite onto the pyroxene- garnet plane. Numbered circles refer to oxide mix compositions given in Table 1; Mix 31 indicated by the open circle is multiply saturated in all crystalline phases [L + Fo + Opx + Cpx + Gt]. Bounding data at 10 GPa on the joins Diopside-Enstatite and Enstatite-Pyrope are from Gasparik (1992, 1996). Inset shows the effect of adding 1 wt% of each oxide to the invariant point.

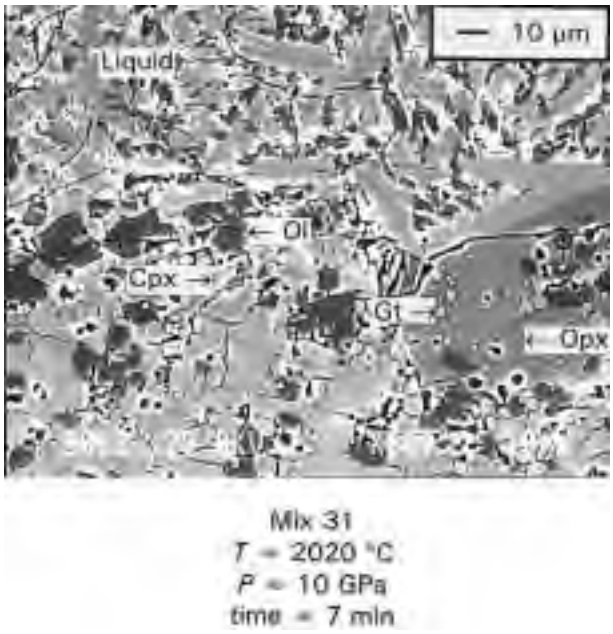

FIGURE 2. Backscatter scanning electron microscope image of an experiment on mix 31. Liquid quenches to quench clinopyroxenes and olivines. Olivine, orthopyroxene, clinopyroxene, and garnet are all in contact with liquid.

ated with the electron microprobe analysis of the liquid phase quenched in simple chemical systems (Herzberg and Zhang 1997). Liquids with komatiite analogue compositions in the system CMAS do not quench to glass, but to a complex intergrowth of olivine and clinopyroxene. The sizes and proportions of olivine and clinopyroxene vary with bulk composition, and for liquids at invariant points, the quench olivine crystals tend to be small and imbedded in much larger crystals of quench clinopyroxene. Polished electron probe mounts tend to have a high crack density with severe plucking of olivine and clinopyroxene (Herzberg and Zhang 1997). This invariably results in electron microprobe totals that range from 95 to 97%, and normalization to 100% is problematic because the analysis is biased toward the phase that is most resistant to plucking, this being clinopyroxene. The addition of 10% FeO to experimental compositions reduces the size of the quench crystals and can almost eliminate cracks completely, resulting in good analyses with totals equal to 100 ± 1 wt% (Herzberg and Zhang 1997).

Another important problem is the effect of temperature gradients in assemblies with straight heaters. There are advantages and disadvantages to using this technique, and the reader is referred to the extensive discussion reported elsewhere (Herzberg et al. 1990; Herzberg 1992; Zhang and Herzberg 1994; Herzberg and Zhang 1996, 1997). The temperature gradient in the hot spot of these experiments is typically 50 °C/mm, and this can be reduced to 25 °C/mm with stepped heaters (Walter 1998). It is never entirely eliminated, and the chief effect is to cause thermal migration of the liquid phase from the cold to hot areas of the sample by a dissolution and precipitation process. This is the greatest source of uncertainty in determining the composition of the liquid phase at the 10 GPa invariant point, and its magnitude is estimated below.

Time series experiments at 7 to 60 min and 5 GPa showed no change in the identity of the liquidus phase and no change in absolute oxide abundances or in FeO-MgO partitioning between crystals and liquid (Herzberg and Zhang 1997). Reversals were achieved in the sense of observing simultaneous solution and precipitation of the liquidus phases over the length of the temperature gradient (Walker and Agee 1989; Herzberg et al. 1990;

TABLE 3. Electron microprobe analyses of coexisting phases at 10 GPa (this work) and 5 GPa (Herzberg and Zhang 1997) (wt%)

	No. of analyses	SiO_2	Al_2O_3	MgO	CaO	Total
Liquid—5 GPa*		48.85(0.18)	9.55(0.13)	30.90(0.30)	10.70(0.15)	100.00
Fo—5 GPa*	9	42.43(0.43)	0.21(0.01)	57.02(0.37)	0.31(0.02)	99.97
Opx—5 GPa*	35	57.20(0.50)	3.58(0.60)	36.04(0.44)	3.07(0.27)	99.89
Cpx—5 GPa*	58	55.80(0.64)	3.78(0.72)	30.62(1.29)	9.49(1.39)	99.69
Gt—5 GPa*	49	44.11(0.42)	24.60(0.44)	25.71(0.62)	5.58(0.68)	100.00
Liquid—10 GPa†		51.40(0.20)	3.77(0.43)	36.60(0.25)	8.23(0.52)	100.00
Fo—10 GPa†	3	43.04(0.20)	0.14(0.01)	56.45(0.42)	0.25(0.02)	99.88
Opx—10 GPa†	13	59.48(0.61)	0.99(0.10)	37.46(0.47)	2.55(0.16)	100.48
Cpx—10 GPa†	16	58.70(0.42)	0.99(0.02)	33.25(0.72)	7.53(0.64)	100.48
Gt—10 GPa†	9	47.80(0.54)	19.93(0.51)	28.18(0.48)	4.80(0.40)	100.71

Note: Numbers in parentheses equal 1σ for crystalline phases and 2σ for liquid phases.
* Herzberg and Zhang (1997).
† Liquid—10 GPa = oxide mix 31; crystalline phases from mix 31-experiment 1.

Zhang and Herzberg 1994; Herzberg and Zhang 1996, 1997), but polythermal melting and precipitation reversals were not performed.

EXPERIMENTAL RESULTS

Listed in Table 1 are the compositions of the mixed oxide starting materials in both the CMAS and MS systems. The phase equilibrium results of experiments conducted on these starting materials at 10 GPa are listed in Table 2 and illustrated in Figures 1a and 1b. Three experiments reported previously at 10 GPa are included (i.e., mixes C, C67, and C50; Herzberg et al. 1990; Herzberg 1992), and are in excellent agreement with the present work.

Figures 1a and 1b are projections of the liquidus crystallizations fields for forsterite, orthopyroxene, clinopyroxene, and garnet together with their bounding cotectics. The 10 GPa invariant point has been determined precisely by mix 31, which shows multiple saturation in these four crystalline phases [L + Fo + Opx + Cpx + Gt], as seen in Figure 2. The liquid at this invariant point was estimated previously to have the composition of mix 27 (Herzberg 1992). We tested this estimate by preparing and running an experiment on mix 27 and found that it is saturated in garnet only [L + Gt]; forsterite, orthopyroxene, and clinopyroxene crystallize about 20 °C lower, so this composition is almost multiply saturated in garnet lherzolite. Although mix 27 is very similar to our new and preferred peritectic liquid composition 31 as seen in Table 1, the ''shotgun'' technique is highly successful in resolving subtle phase equilibrium responses to small changes in bulk composition. Mix 31 differs from mixes 27 and 32 by $\pm 0.20\%$ SiO_2, $\pm 0.43\%$ Al_2O_3, $\pm 0.25\%$ MgO, and $\pm 0.52\%$ CaO. With essentially negligible uncertainties arising from weighing oxide components (Herzberg and Zhang 1997), these differences in bulk composition are a good indication of the uncertainty arising from the brackets of the ''shotgun'' technique.

The most important source of uncertainty results from systematic differences between quench liquid and oxide mix compositions owing to thermal migration of liquid in the temperature gradient. We were able to evaluate this difference with experiments in the system CaO-MgO-FeO-Al_2O_3-SiO_2 at 5 GPa because Fe was found to reduce the size of the quench crystals and eliminate cracks, and render it possible to analyze the experimental change accurately with the electron microprobe (Herzberg and Zhang 1997). Near the invariant point, the differences between oxide mix and quench liquid compositions in absolute weight percent are: $SiO_2 = +0.15$; $Al_2O_3 = +0.11$; FeO = −1.01; MgO = +1.08; CaO = −0.38. Down the temperature gradient, Opx is not stable and the experimental samples consist of an assemblage of olivine, clinopyroxene, and garnet [i.e., L + Ol + Cpx + Gt]; the addition of a small amount of this liquid to the larger pool of analyzed liquid at the hot spot by thermal migration will lower SiO_2 and MgO and elevate FeO, thereby accounting for the differences between oxide and analyzed liquid compositions. The problem with extending these uncertainties to CMAS is that the addition of FeO to CMAS widens the temperature interval between the solidus and liquidus, and this contributes a greater amount of liquid during thermal migration. Uncertainties in the absolute error in the 10 GPa peritectic liquid composition are thus: $SiO_2 = \pm 0.20$ to 0.25%; $Al_2O_3 = \pm 0.43$ to 0.44%; MgO = ± 0.25 to 1.11%; CaO = ± 0.52 to 0.64%. The minimum bound is based on uncertaintes from the ''shotgun'' method, and the maximum bound is estimated by a summation of the squares of uncertainties arising from the ''shotgun'' method and the effects of thermal migration in FeO-bearing systems at 5 GPa. In general, experiments in a temperature gradient become more problematic as the bulk composition becomes increasingly different from the peritectic liquid composition. For melting experiments on peridotite bulk compositions, the effects of thermal migration are much greater than those documented here (Herzberg and Zhang 1996). A superior method for examining low melt fractions in peridotite compositions involves minimizing temperature gradients with stepped heaters (Walter 1998).

The compositions of coexisting forsterite, orthopyroxene, clinopyroxene, and garnet in mix 31 were determined by wavelength dispersive electron microprobe analysis using an analytical method described previously (Herzberg and Zhang 1997); the results are listed in Table 3 and projected in Figure 1b. It can be seen that the melting of garnet lherzolite at 10 GPa is peritectic, similar to what we observe at 5 GPa (Herzberg and Zhang 1997). Melting coefficients for these reactions are:

$$0.12\ \text{Fo} + 0.70\ \text{Cpx} + 0.18\ \text{Gt} = 0.61\ \text{L} + 0.39\ \text{Opx} \quad (1)$$

at 5 GPa (Herzberg and Zhang 1977), and

$$0.18\ \text{Fo} + 0.72\ \text{Cpx} + 0.10\ \text{Gt} = 0.59\ \text{L} + 0.41\ \text{Opx} \quad (2)$$

at 10 GPa. The drop in the coefficient for garnet with increasing pressure reflects a reduction in the solubility of garnet in the liquid; similarly, the increase in the coefficient for forsterite with pressure reflects a small increase in the solubility of forsterite in the melt phase. The effect of pressure on the compositions of liquids formed by the melting of a garnet lherzolite analogue [L + Fo + Opx + Cpx + Gt] is shown more clearly in Figures 3a and 3b.

Pressure causes the primary crystallization field of garnet to expand at the expense of all other crystalline phases, and this can yield liquids with very low contents of Al_2O_3 (Figs. 3a and 3b; see also Herzberg 1992, 1995; Walter 1998). Our data at 5 and 10 GPa show that the increase in the amount of normative forsterite is actually very small, whereas there is a substantial increase in normative enstatite (Figs. 3a and 3b). This increase in normative enstatite is not evident by casual inspection of the reaction coefficients in Equations 1 and 2, but becomes clear when a comparison is made with pyroxene and garnet phase compositions at 5 GPa and 10 GPa (Table 3; Fig. 3b). Pressure imposes a reduction in Al_2O_3 and an increase in SiO_2 in these crystalline phases, and this is reflected in the liquid. Indeed, the lowest content of SiO_2 in magmas generated by the partial melting of garnet lherzolite occurs at the spinel- to garnet-lherzolite transition, and the effect of pressure is to generate increasingly siliceous liquids (Herzberg 1992). The pressure-induced peritectic liquid track shown in Figure 3a exhibits substantial curvature, which results in a maximum in normative forsterite content at about 8 GPa.

A forsterite maximum seen for peritectic liquids in CMAS can also be observed in the simple binary forsterite (Mg_2SiO_4)-enstatite ($Mg_2Si_2O_6$), as illustrated in Figure 4. Melting is eutectic at high pressures, and we were able to bracket this liquid by observing the liquidus phases for several compositions at various pressures; the results of these experiments are included in Table 2. The effect of pressure on the amount of normative forsterite in the liquid is most evident between 1 atmosphere and 5 GPa, but at higher pressures the behavior is complicated. Again, a maximum occurs at 7 to 8 GPa, and at higher pressures the forsterite content of the eutectic actually drops until it reaches a minimum at around 11.5 GPa

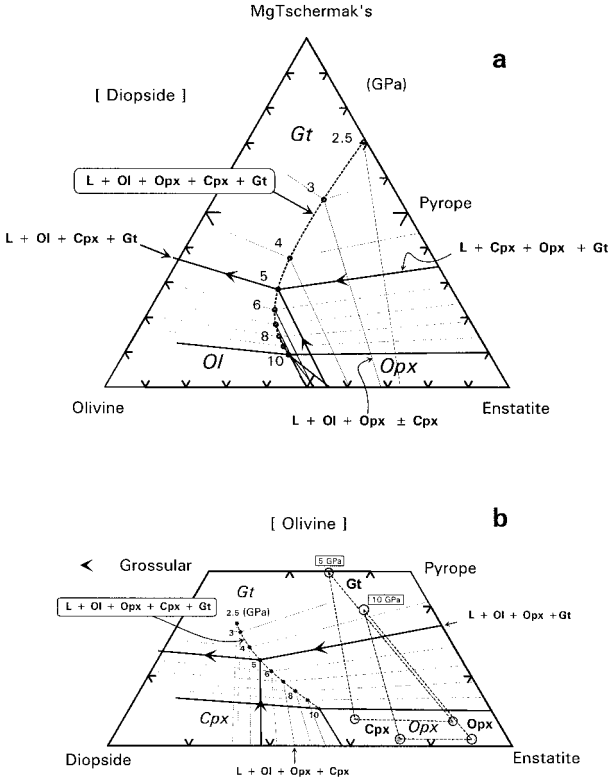

FIGURE 3. The effect of pressure on liquidus crystallization fields, cotectic boundaries, and invariant points. Bold phase boundaries at 10 GPa are from Figures 1a and 1b; bold phase boundaries at 5 GPa are from Herzberg and Zhang (1997). Broken curve = compositions of liquids coexisting with garnet peridotite [L + Fo + Opx + Cpx + Gt] at the pressures indicated in GPa; interpolated compositions are anchored to the spinel- to garnet-peridotite transition at about 2.5 GPa (Herzberg and O'Hara unpublished manuscript), and can be retrieved from the following empirical equations:

$$\text{CaO (wt\%)} = 10.04 - 0.2853P + 10.43/P$$

$$\text{MgO (wt\%)} = 37.10 + 0.3467P - 39.67/P$$

$$\text{Al}_2\text{O}_3\ \text{(wt\%)} = 6.21 - 0.546P + 30.4/P$$

$$\text{SiO}_2\ \text{(wt\%)} = 46.85 + 0.4733P - 1.83/P.$$

Light lines labeled [L + Fo + Opx ± Cpx] are fixed by eutectics on the forsterite-enstatite binary (see below) and may or may not be saturated in clinopyroxene. All other light lines are inferred cotectic boundaries. Italicized Gt, Cpx, and Opx are liquidus crystallization fields. Unitalicized Gt, Cpx, and Opx are crystalline phase compositions at 5 and 10 Gpa.

where orthoenstatite transforms to the clinoenstatite structure (Pacalo and Gasparik 1990). For the eutectic melting of forsterite and orthoenstatite, we have fitted our experimental brackets to the lower pressure data of Bowen and Andersen (1914) and Liu and Presnall (1990) with the following empirical equation:

$$\text{SiO}_2\ \text{(wt\%)} = 60.94 - 2.209P + 0.1486P^2 \quad (3)$$

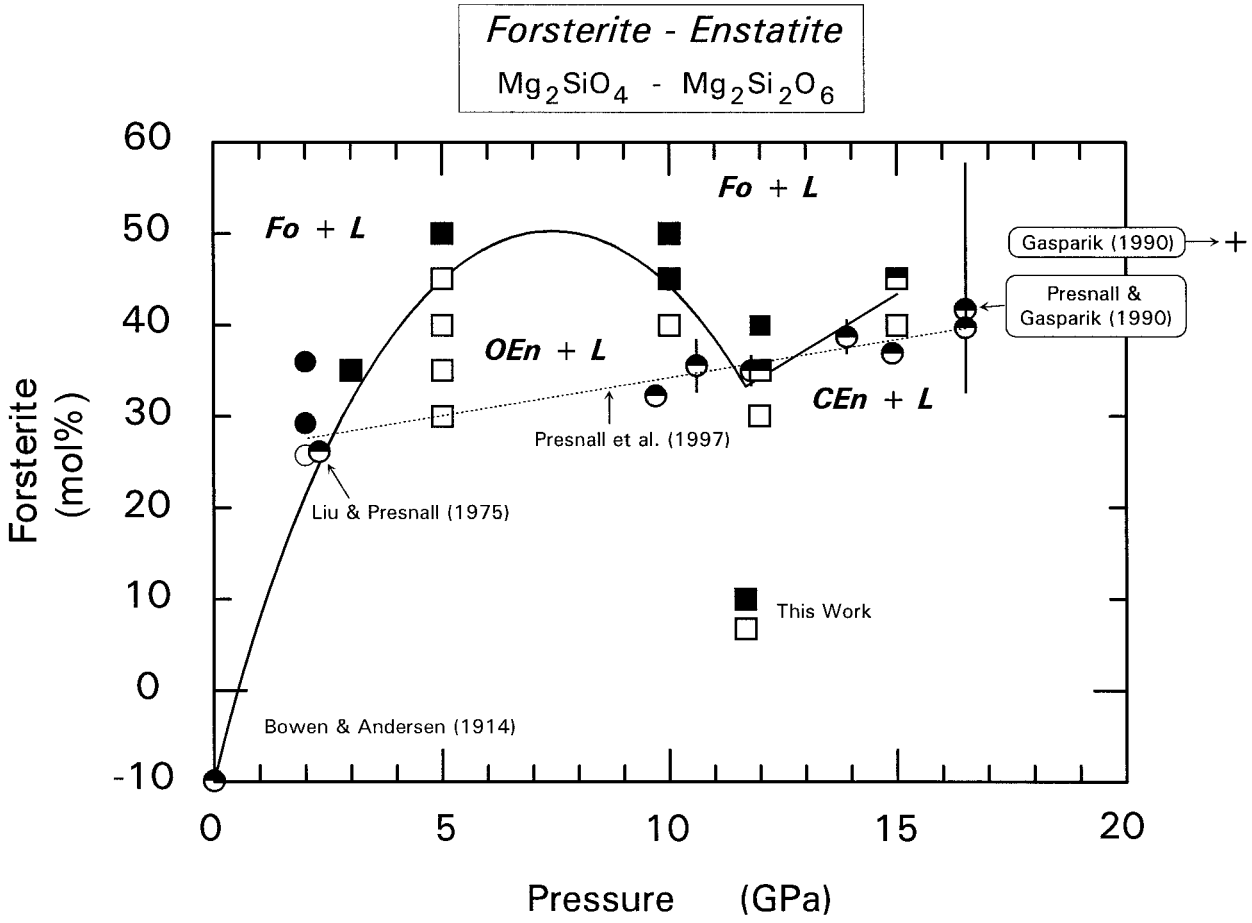

FIGURE 4. The effect of pressure on eutectic liquid compositions for the binary system Forsterite-Enstatite. Squares = oxide mixes in Table 1; closed square = liquidus forsterite; open square = liquidus enstatite. Circles = eutectic and peritectic liquids determined by Bowen and Andersen (1914), Liu and Presnall (1990), Gasparik (1990), Presnall and Gasparik (1990), and Presnall et al. (1998).

In the 5 to 10 GPa range, our observed eutectic liquids have higher forsterite contents than those inferred by Presnall et al. (1998) from interpolation of their 2.0 and 9.7 GPa end points (Fig. 4). However, there is very good agreement at pressures above about 12 GPa (Presnall and Gasparik 1990; Presnall et al. 1998).

DISCUSSION

When the lithosphere is passively stetched, it is replaced by upwelling asthenospheric mantle that can partially melt at about 0.2 to 3.0 GPa, yielding liquids that are similar to basaltic magmas (e.g., O'Hara 1968; McKenzie and Bickle 1988; Langmuir et al. 1992). But when mantle peridotite ascends in a hot plume, it tends to melt at higher pressures, possibly as high as 8 to 9 GPa (Herzberg 1992). Because the adiabatic gradient of the plume has a smaller dT/dP than the solidus, progressive melting must take place (McKenzie and Bickle 1988), and it is important to understand the polybaric geochemical evolution of these magmas.

Plagioclase- and spinel-lherzolite are the peridotite assemblages melted from 1 atmosphere to about 2.5 GPa. But at higher pressures where garnet is stable, orthopyroxene can be absent from melting on the solidus because it can be completely dissolved in the clinopyroxene (Herzberg and Zhang 1996; Walter 1998). We use our experimental results at 5 to 10 GPa to illustrate this point in Figure 5. A range of naturally occurring, pyrolite-like peridotite compositions have been projected from olivine onto the pyroxene-garnet plane. These contain MgO in the 36 to 42% range and, in general, the more refractory mantle projects to higher normative enstatite. It can be seen that, with one exception, mantle peridotite crystallizes to the subsolidus mineralogy [Ol + Cpx + Gt], and the melting of this assemblage must be Opx-free [L + Ol + Cpx + Gt]. The solidus is defined by [L + Ol + Cpx + Gt], and liquids formed by advanced melting along this cotectic become increasingly enriched in SiO_2. These Opx-free initial melting assemblages were not observed by Herzberg and Zhang (1996) because of the large ther-

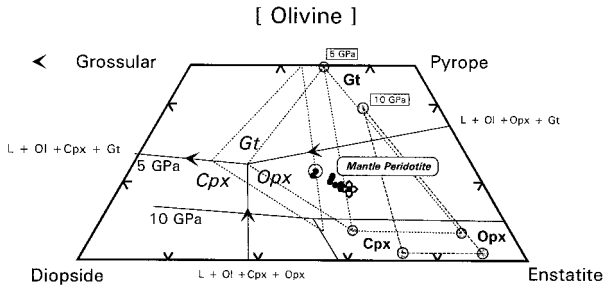

FIGURE 5. A projection from olivine of 5 and 10 GPa cotectic equilibria, coexisting pyroxenes and garnet, and mantle peridotite (closed circles). Broken lines = lines connecting coexisting crystalline + liquid phases. Initial melting of Opx-free assemblage [L + Ol + Cpx + Gt] at 5 GPa is illustrated for the peridotite composition indicated as a circle within a circle. Initial melting of Opx-bearing garnet lherzolite [L + Ol + Opx + Cpx + Gt] at 5 GPa is illustrated for the peridotite composition indicated as a circle within a cross; at 10 GPa the solidus assemblage is Opx-free. The effect of FeO is to increase the prospects for Opx-free initial melting because it increases the solubility of En in Cpx and restricts the range of peridotite compositions that project into the triangle defined by Cpx-Opx-Gt (Herzberg and Zhang 1997). Peritectic melt compositions are from Table 3.

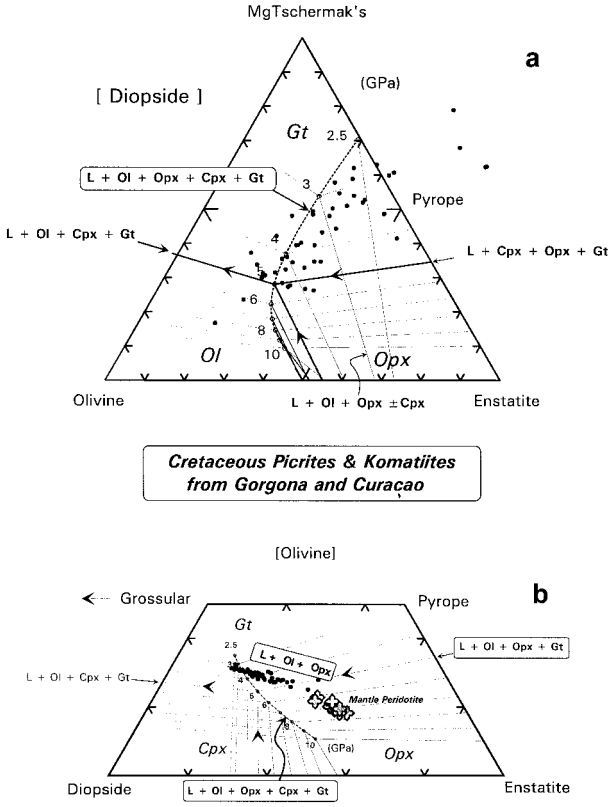

FIGURE 6. Projections of Gorgona and Curaçao picrites and komatiites. **(a)** From Diopside onto the plane Olivine-Enstatite-MgTschermak's. (**b)** From Olivine onto the garnet-pyroxene plane. Closed circles = picrites and komatiites with higher degree melts having higher normative enstatite; Filled crosses = mantle peridotites with more refractory types having higher normative enstatite; the trend is genetically independent of the trend of picrites and komatiites. Invariant points and cotectics are from Figure 3. Data sources are cited in the text. The effects of TiO_2, Cr_2O_3, Na_2O, and K_2O are small but included in the projection code (Herzberg and O'Hara unpublished manuscript).

mal gradients in their experiments, but they were confirmed to exist by Walter (1998). When the degree of melting is elevated even more, Opx is stabilized by the reaction Ol + Cpx + Gt = L + Opx (Davis and Schairer 1965; O'Hara and Yoder 1967; Herzberg 1992; Herzberg et al. 1990; Herzberg and Zhang 1997; Longhi 1995; Kinzler 1997; Walter 1998) and melting will once again involve garnet lherzolite [L + Ol + Opx + Cpx + Gt]. The melt composition in this scenario depends critically on the composition of the source peridotite. Figure 5 shows that at 5 GPa initial melting can be peritectic and involve Opx for more refractory mantle, which is enriched in enstatite [L + Ol + Opx + Cpx + Gt], but at 10 GPa it is Opx-free [L + Ol + Cpx + Gt].

For most peridotite compositions, progressive isobaric melting at 3.5 to 8 GPa eliminates crystalline phases in the following order: [L + Ol + Opx + Gt) $\rightarrow$ (L + Ol + Opx] $\rightarrow$ (L + Ol). The same progressive melting sequence can also occur polybarically by decompression in an ascending hot plume, and the magmas that erupt are typically komatiites and picrites (MgO $\geq$ 18 wt%; Herzberg 1992). In the discussion that follows, naturally occurring komatiites are compared with the experimentally constrained cotectic phase relations in the system CMAS. The addition of FeO to this simple system expands the liquidus crystallization field of garnet at the expense of all other crystalline phases by a small amount, and this has been calibrated experimentally at 5 GPa for FeO contents that range from 11 to 17 wt% (Herzberg and Zhang 1997). The application of liquidus phase relations in the system CMAS to komatiites that typically contains 11% FeO results in an error that is roughly the same as the size of the experimental uncertainties discussed above. Phase equilibria in the system CMAS therefore provide an excellent description of melting and crystallization of komatiites at high pressures.

Komatiites and picrites of Cretaceous age from Gorgona and Curaçao (Echeverria 1982; Aitken and Echeverria 1984; Echeverria and Aitken 1986; Kerr et al. 1996a, 1996b; Arndt et al. 1997) are thought to have melted in a plume that gave rise to the Carribean plateau (Storey et al. 1991). Projections of these data demonstrate that their compositions are dominated by the addition and subtraction of olivine, which is observed to occur at the surface, and this appears as the strong olivine control in Figure 6a. By projecting from olivine, we can filter through this surficial olivine control signature, and the results are seen in Figure 6b. Now a strong enstatite control is observed emanating from mantle peridotite, demonstrating that the parental komatiite compositions are

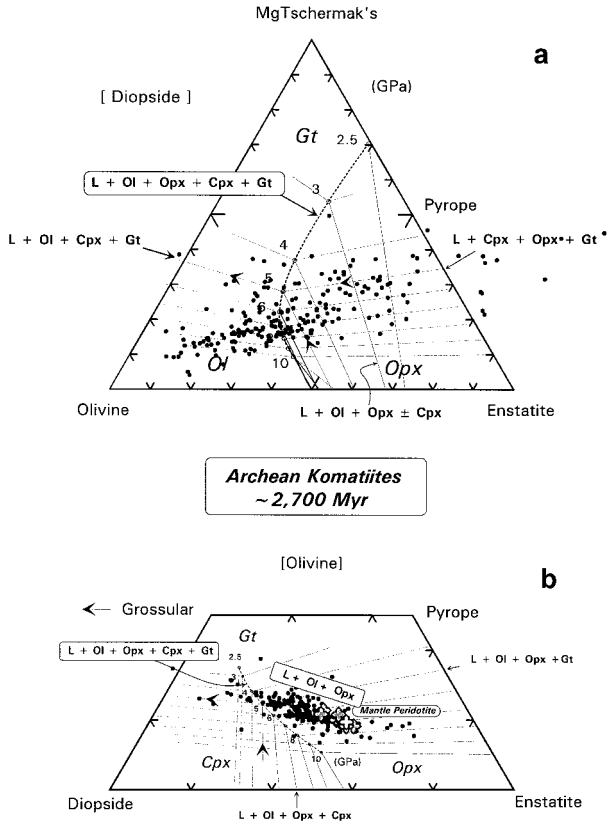

FIGURE 7. Projections of 2700 Myr Archaean komatiites from all cratons. **(a)** From Diopside onto the plane Olivine-Enstatite-MgTschermak's. (**b)** From Olivine onto the garnet-pyroxene plane. Data sources are cited in Herzberg (1992, 1995). Invariant points and cotectics are from Figure 3. The effects of TiO_2, Cr_2O_3, Na_2O, and K_2O are small but included in the projection code (Herzberg and O'Hara unpublished manuscript).

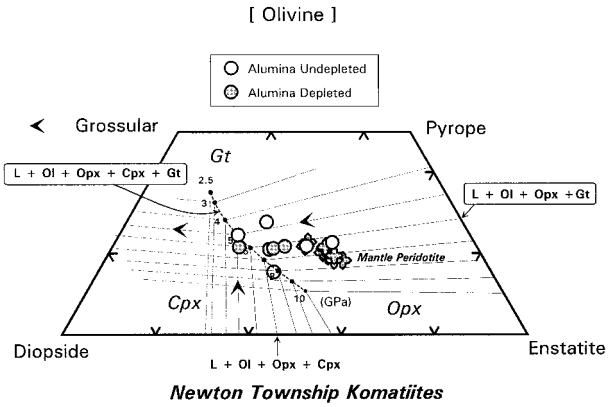

FIGURE 8. A projection of 2700 Myr komatiites from the Newton Township, Ontario (Cattell and Arndt 1987). Alumina-depleted komatiites are generally elevated in Diopside-Garnet, but the sample with the highest Diopside-Garnet is actually a high-MgO, olivine-porphyritic, alumina-undepleted komatiite (no. 15 of Cattell and Arndt 1987), and is most likely to be an altered sample that experienced CaO addition. Invariant points and cotectics are from Figure 3. The effects of TiO_2, Cr_2O_3, Na_2O, and K_2O are small but included in the projection code (Herzberg and O'Hara unpublished manuscript).

dominated by harzburgite (L + Opx + Ol), a conclusion reached previously (Herzberg 1992, 1995; Herzberg and O'Hara unpublished manuscript).

Komatiites with 2700 Myr Archaean ages are the alumina-undepleted types of Nesbitt et al. (1979), and these have been projected in Figure 7. This is a global database of komatiites from all cratons (Herzberg 1992, 1995), and the strong harzburgite control is still evident (Fig. 7b). The projected compositions exhibit substantial scatter in Diopside/Pyrope, which is likely to arise both from alteration and from variations in peridotite source chemistry (Herzberg 1992). Indeed, it can be seen in Figure 7b that almost all of the dispersion in the data can be attributed to variations in CaO-Al_2O_3 for mantle peridotite (see also Herzberg 1995).

An exception to the rule of harzburgite control is represented by the occurrence of both alumina-undepleted and alumina-depleted komatiites from a single locality in the Newton Township of Ontario (Cattell and Arndt 1987), which are shown here in Figure 8. The alumina-depleted types are highest in Diopside/Pyrope, depleted in heavy rare earth elements (HREE), and have low Al_2O_3-TiO_2, indicating the involvement of garnet (Cattell and Arndt 1987). Figure 8 shows that these komatiites are roughly coincident with liquids that could have formed by variable degrees of melting of a garnet harzburgite assemblage (L + Ol + Opx + Gt). Another interpretation is that mixing could have occurred between liquids with residual harzburgite and liquids extracted from garnet lherzolite by lower degrees of melting. The Tertiary picrites from West Greenland also display a garnet harzburgite signature (Herzberg and O'Hara unpublished manuscript), which indicates that the Icelandic plume from which they formed (Holm et al. 1993) had a lower potential temperature than most plumes.

Most komatiites with Cretaceous and late-Archaean ages are not coincident in projection with any of the following peridotite melting assemblages: [L + Ol + Cpx + Gt], [L + Ol + Opx + Cpx + Gt], or [L + Ol + Opx + Gt] except by chance. These observations illustrate that garnet and clinopyroxene are usually melted out during decompression melting of peridotite in hot plumes, and when this occurs, further melting involves a residual harzburgite mineralogy [L + Ol + Opx]. The inference of a harzburgite residuum is consistent with trace elements, which show no depletions in HREE that can be attributed to residual or cumulate garnet (Arndt et al. 1997; Bickle et al. 1993). However, there is an important caveat to this interpretation. The harzburgite signature observed in projection has been interpreted above as the product of a partial melting process, but partial crystallization of komatiite liquids saturated in olivine-orthopyroxenite [L + Ol + Opx] by heat exchange with a cold lithosphere could give rise to derivative liquids with vari-

able normative enstatite, and in projection these would be indistinguishable from liquids formed by variable degrees of partial melting. Partial crystallization can yield derivative liquids that are modestly enriched in FeO compared to partial melts, but these cannot be distinguished easily from liquids produced by the partial melting of an Fe-rich peridotite source (Herzberg and O'Hara unpublished manuscript). The only requirement for the partial crystallization interpretation is that it involve liquids formed by high degrees of partial melting, with either a harzburgite residuum [L + Ol + Opx] or an olivine residuum [L + Ol]. This difficult problem has not been resolved adequately and will be the subject of further inquiries.

The amount of orthopyroxene that is melted out of a harzburgite residuum during decompression depends on how hot the ascending plume is. Very hot plumes could conceivably melt all orthopyroxene and have a residuum consisting of olivine [L + Ol]; eruption of these magmas followed by crystallization of olivine at the surface would be manifest in projected komatiites that would coincide with mantle peridotite in the olivine projection of Figure 7b. This is certainly a possibility for some komatiites (Fig. 7b), although the harzburgite control generally dominates. A residual harzburgite signature for most komatiites with Cretaceous and late-Archaean ages has been interpreted to have formed by about 25 to 60% anhydrous melting of mantle peridotite and in plumes with potential temperatures that were 200 to 400 °C higher than those of present-day oceanic ridges (Herzberg 1992, 1995; Nisbet et al. 1993; Abbott et al. 1994; Walter 1998; Herzberg and O'Hara unpublished manuscript). The phase equilibrium results reported here provide a foundation for exploring in greater detail other problems such as depths of melting and melt segregation, specific source compositions, the effect of plume shape and magma mixing on komatiite geochemistry, the role of partial crystallization of komatiites in the lithosphere, and the importance of komatiites in understanding the origin of cratonic mantle (Herzberg and O'Hara unpublished manuscript).

Acknowledgments

This research was supported by a grant from the National Science Foundation to Claude Herzberg (EAR-9406976). Thanks are extended to Connie Bertka, Robert Dymek, Don Francis, and Ken Windom for their comments. The high-pressure experiments were performed at the Stony Brook High Pressure Laboratory, which is part of the NSF Science and Technology Center for High Pressure Research (EAR-8920239). This is Mineral Physics Publication no. 200 at the Department of Earth and Space Sciences.

References cited

Abbott, D., Burgess, L., and Longhi, J. (1994) An empirical thermal history of the Earth's upper mantle. Journal of Geophysical Research, 99, 13835–13850.

Aitken, B.G. and Echeverria, L.M. (1984) Petrology and geochemistry of komatiites and tholeiites from Gorgona Island, Columbia. Contributions to Mineralogy and Petrology, 86, 94–105.

Arndt, N.T., Kerr, A.C., and Tarney, J. (1997) Dynamic melting in plume heads: the formation of Gorgona komatiites and basalts. Earth and Planetary Science Letters, 146, 289–302.

Bickle, M.J., Arndt, N.T., Nisbet, E.G., Orpen, J.L., Martin, A., Keays, R.R., and Renner, R. (1993). Geochemistry of the igneous rocks of the Belingwe greenstone belt: alteration, contamination and petrogenesis. In M.J. Bickle and E.G. Nisbet, Eds., The Geology of the Belingwe Greenstone Belt, Zimbabwe, p. 175–213. Balkema Press, Rotterdam.

Bowen, N.L. and Andersen, O. (1914) The binary system MgO-SiO_2. American Journal of Science, 4th series, 37, 487–500.

Cattell, A. and Arndt, N. (1987) Low- and high-alumina komatiites from a Late Archaean sequence, Newton Township, Ontario. Contributions to Mineralogy and Petrology, 97, 218–227.

Davis, B.T.C. and Schairer, J.F. (1965) Melting relations in the join diopside-forsterite-pyrope at 40 kilobars and at one atmosphere. Carnegie Institution of Washington, Yearbook, 64, 123–126.

Echeverria, L.M. (1982) Komatiites from Gorgona Island, Columbia. In N.T. Arndt and E.G. Nisbet, Eds., Komatiites, p. 199–209. George Allen and Unwin, London.

Echeverria, L.M. and Aitken, B.G. (1986) Pyroclastic rocks: another manifestation of ultramafic volcanism on Gorgona Island, Columbia. Contributions to Mineralogy and Petrology, 92, 428–436.

Gasparik, T. (1990) Phase relations in the transition zone. Journal of Geophyiscal Research, 95, 15751–15769.

———(1992) Melting experiments on the enstatite-pyrope join at 80–152 kbar. Journal of Geophysical Research, 97, 15181–15188.

———(1996) Melting experiments on the enstatite-diopside join at 70–224 kbar, including the melting of diopside. Contributions to Mineralogy and Petrology, 124, 139–153.

Herzberg, C. (1992) Depth and degree of melting of komatiites. Journal of Geophysical Research, 97, 4521–4540.

———(1995) Generation of plume magmas through time: an experimental perspective. Chemical Geology, 126, 1–16.

Herzberg, C. and Zhang, J. (1996) Melting experiments on anhydrous peridotite KLB-1: compositions of magmas in the upper mantle and transition zone. Journal of Geophysical Research, 101, 8271–8295.

———(1997) Melting experiments on komatiite analogue compositions at 5 GPa. American Mineralogist, 82, 354–367.

Herzberg, C., Gasparik, T., and Sawamoto, H. (1990) Origin of mantle peridotite: constraints from melting experiments to 16.5 GPa. Journal of Geophysical Research, 95, 15779–15803.

Holm, P.M., Gill, R.C.O., Pedersen, A.K., Larsen, J.G., Hald, N., Nielsen, T.F.D., and Thirlwall, M.F. (1993) The Tertiary picrites of West Greenland: contributions from 'Icelandic' and other sources. Earth and Planetary Science Letters, 115, 227–244.

Kerr, A.C., Marriner, G.F., Arndt, N.T., Tarney, J., Nivia, A., Saunders, A.D., and Duncan, R.A. (1996a) The petrogenesis of Gorgona komatiites, picrites and basalts: new field, petrographic and geochemical constraints. Lithos, 37, 245–260.

Kerr, A.C., Tarney, J., Marriner, G., Klaver, G.T., Saunders, A.D., and Thirlwall, M.F. (1996b) The geochemistry and petrogenesis of the late-Cretaceous picrites and basalts of Curaçao, Netherlands Antilles: a remnant of an oceanic plateau. Contributions to Mineralogy and Petrology, 124, 29–43.

Kinzler, R.J. (1997) Melting of mantle peridotite at pressures approaching the spinel to garnet transition: Application to mid-ocean ridge basalt petrogenesis. Journal of Geophysical Research, 102, 853–874.

Langmuir, C.H., Klein, E.M., and Plank, K. (1992) Petrology systematics of mid-ocean ridge basalts: constraints on melt generation beneath ocean ridges. Mantle flow and melt generation at mid-ocean ridges. American Geophysical Union Monograph, 71, 183–280.

Liu, T.-C. and Presnall, D.C. (1990) Liquidus phase relationships on the join anorthite-forsterite-quartz at 20 kbar with applications to basalt petrogenesis and igneous sapphirine. Contributions to Mineralogy and Petrology, 104, 735–742.

Longhi, J. (1995) Liquidus equilibria of some primary lunar and terrestrial melts in the garnet stability field. Geochimica Cosmochimica Acta, 59, 2375–2386.

McKenzie, D. and Bickle, M.J. (1988) The volume and composition of melt generated by extension of the lithosphere. Journal of Petrology, 29, 625–679.

Nesbitt, R.W., Sun, S.-S., and Purvis, A.C. (1979) Komatiites: geochemistry and genesis. Canadian Mineralogist, 17, 165–186.

Nisbet, E.G., Cheadle, M.J., Arndt, N.T., and Bickle, M.J. (1993) Constraining the potential temperature of the Archaean mantle: a review of the evidence from komatiites. Lithos, 30, 291–307.

O'Hara, M.J. (1968) The bearing of phase equilibria studies in synthetic and natural systems on the origin of basic and ultrabasic rocks. Earth Science Reviews, 4, 69–133.

O'Hara, M.J. and Yoder, H.S., Jr. (1967) Formation and fractionation of basic magmas at high pressures. Scottish Journal of Geology, 3, 67–117.

Pacalo, R.E.G. and Gasparik, T. (1990) Reversals of the orthoenstatite-clinoenstatite transition at high pressures and high temperatures. Journal of Geophysical Research, 95, 15853–15858.

Presnall, D.C. and Gasparik, T. (1990) Melting of enstatite ($MgSiO_3$) from 10 to 16.5 GPa and the forsterite (Mg_2SiO_4)-majorite ($MgSiO_3$) eutectic at 16.5 GPa: implications for the origin of the mantle. Journal of Geophysical Research, 95, 15771– 15777.

Presnall, D.C., Weng, Y.-H., Milholland, C.S., and Walter, M.J. (1998) Liquidus phase relations in the system MgO-$MgSiO_3$ at pressures up to 25 GPa: Constraints on crystallization of a molten Hadean mantle. Physics of the Earth and Planetary Interiors, in press.

Storey, M., Mahoney, J.J., Kroenke, L.W., and Saunders, A.D. (1991). Are oceanic plateaus sites of komatiite formation? Geology, 19, 376–379.

Walker, D. and Agee, C. (1989) Partitioning ''equilibrium,'' temperature gradients, and constraints on Earth differentiation. Earth and Planetary Science Letters, 96, 49–60.

Walter, M.J. (1998) Melting of garnet peridotite and the origin of komatiite and depleted lithosphere. Journal of Petrology, 39, 29–60.

Zhang, J. and Herzberg, C. (1994). Melting experiments on anhydrous peridotite KLB-1 from 5.0 to 22.5 GPa. Journal of Geophysical Research, 99, 17729–17742.

Manuscript received September 26, 1997
Manuscript accepted January 3, 1998
Paper handled by Robert F. Dymek